# RSC Advances

ROYAL SOCIETY
OF **CHEMISTRY**

www.rsc.org/advances

Journal Name

RSC Advances

Dynamic Article Links▶

**ARTICLE TYPE**

# Hydrothermal synthesis of uniformly dispersed hybrid graphene-TiO$_2$ nanostructure for optical and enhanced electrochemical application

**Rajesh Kumar,\*$^{a,b}$ Rajesh Kumar Singh,\*$^c$ Pawan Kumar dubey,$^d$ Dinesh Pratap Singh,$^e$ Ram Manohar Yadav,$^f$ and Radhey Shyam Tiwari $^b$**

Highly dispersed TiO$_2$ nanoparticles on the graphene nanosheets were achieved by hydrothermal treatment of graphite oxide powder obtained by modified Hummer's method. Hybrid graphene TiO$_2$ nanostructures composite (H-GTN) showed enhanced optical and electrochemical properties for future application as a supercapacitor. The structural, optical and electrochemical properties of these composite are systematically investigated. As prepared H-GTN showed quenching phenomenon in the photoluminescence properties, 10 that was attributed to the specific properties of graphene. Remarkably, the CV test as obtained from H-GTN showed very high specific capacitance value up to 530 F/g at a scan rate of 3 mV/s, and nearly stable capacitance of 400 F/g above 20 mV/s. The cyclic stability test shows stable behavior after some initial cycle and the stability retained without obvious aging or performance degradation showing long cyclic stability. This attributed the excellent electrochemical performance of the H-GTN electrode material for practical application 15 in energy storage devices.

## Introduction

Graphene, a monolayer of sp$^2$-hybridized carbon atoms arranged in a two-dimensional honeycomb lattice, has attracted 20 tremendous attention and research in recent years, owing to its exceptional properties such as high thermal conductivity, ultrahigh charge carrier mobility, extremely large surface area, high mechanical strength and flexibility.[1-4] Though free standing graphene has excellent physical, chemical and electrical 25 properties, however its tendency to restack is a major hurdle in realizing its full potential especially in applications such as super capacitors and lithium ion batteries. These aggressive unique properties along with atomic scale dimension offer various potential applications as nanoelectronics, energy 30 conversion/storage, catalyst, and nanocomposites.[5-9] The two dimensional sheet structure of graphene provides an excellent conductive platform for accommodating nanosized electrochemically active materials and allowed to coat the surface while at the same time providing conduction channels for the 35 transport of electrons. In addition, high surface area and high charge carrier mobility of graphene offers new opportunities to develop graphene-based hybrid nanocomposite materials with

other most common metal oxides/hydroxides and conducting polymers for supercapacitor applications.[6, 10]
40 Transition metal oxides have been explored as potential electrode materials for use in supercapacitors with their pseudocapacitance based charge storage mechanisms.[11-14] RuO$_2$ has been found to give high capacitance due to redox transitions that penetrates into the bulk of the material. However, the cost of Ru is one of the 45 major concerns for its commercial acceptance. The use of graphene has been widely explored as the nanoscale substrates for the formation of nanocomposites with metal oxides to obtain a hybrid, which may have combined features of both graphene and nanosized metal oxide particles.[15, 16] In recent years, metal oxides 50 such as TiO$_2$, MnO, RuO, IrO, etc. have been used in graphene-based supercapacitors with the function of contributing pseudo-capacitance to the total capacitance.[17] TiO$_2$ is considered to be one of the most attractive compounds for supercapacitors not only due to its pseudocapacitance properties but due to its 55 abundance in nature, commercial viability, excellent chemical stability, nontoxicity to the atmosphere and high surface area. Therefore, it is necessary to develop a simple and effective method to prepare highly dispersed hybrid graphene-TiO$_2$ nanocomposites (H-GTN) for supercapacitor application.
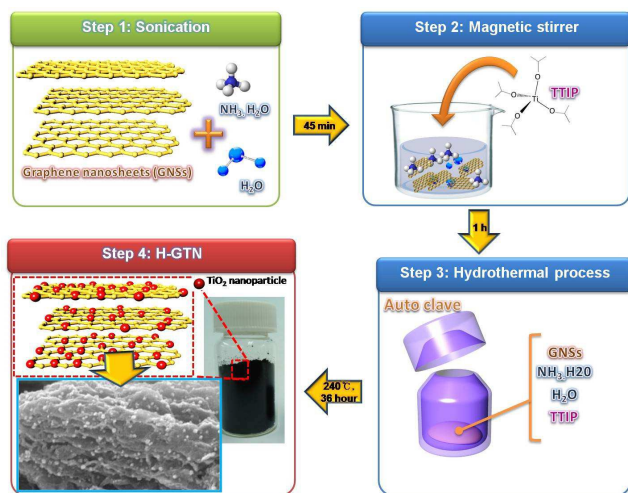
**Fig. 1** Schematic representation for the formation of H-GTN using hydrothermal process Caption

A variety of methods has been demonstrated for the preparation of graphene-TiO$_2$ composite, including chemical, hydrothermal, photo-catalytic methods, and so on.[9, 16, 18, 19] In this work, we report the synthesis of H-GTN using facile hydrothermal method under mild condition and explored their optical and electrochemical properties to elucidate its potential applications as supercapacitor. The H-GTN is synthesized via in-situ hydrothermal process employing titanium tetraisopropoxide (TiC$_{12}$H$_{28}$O$_4$) precursor as titania source. In H-GTN, graphene nanosheets provide a large surface area for the decoration of TiO$_2$ nanostructure and serve as a highly conductive supportive base. Our experimental results show that the hybrid nanostructure

exhibits overall specific capacitance of 400 F/g with high cyclic stability in aqueous electrolyte.

## Result and Discussions

The stepwise schematic in-situ hydrothermal synthesis procedure of H-GTN is shown in Fig 1. As obtained graphene sheets and H-GTN were characterized by SEM for microstructural characterizations. Fig. 2a shows the SEM micrographs of as synthesized GNSs, and H-GTN. Fig. 2a reveals that the GNSs consisting of randomly aggregated, thin crumpled 3-dimensional structure of the sheets closely associated with each other and having disordered structure. The folded regions of the sheets were found to have an average width of ~1µm by high resolution SEM. Fig. 2b shows the attached TiO$_2$ nanoparticles on the wrinkled surface of GNSs. In H-GTN, the TiO$_2$ nanoparticles are attached to the surface of GNSs with the help of oxygen functionalities formerly attached on the graphene surface. At high TiO$_2$ content, it is uniformly decorated and firmly anchored on the wrinkled GNSs layers with uniform density. Energy-dispersive X-ray spectroscopy (EDS) analysis of H-GTN hybrids is shown in the inset of Fig. 2c. This shows the analysis of H-GTN hybrids. The EDS data of H-GTN shows that the elemental content of C,O and Ti only elements detected, indicating that H-GTN has a higher O content. Based on the obtained results, the atomic weight percentages of C, O and Ti were 63.32, 25.16 and 11.51 %, respectively.
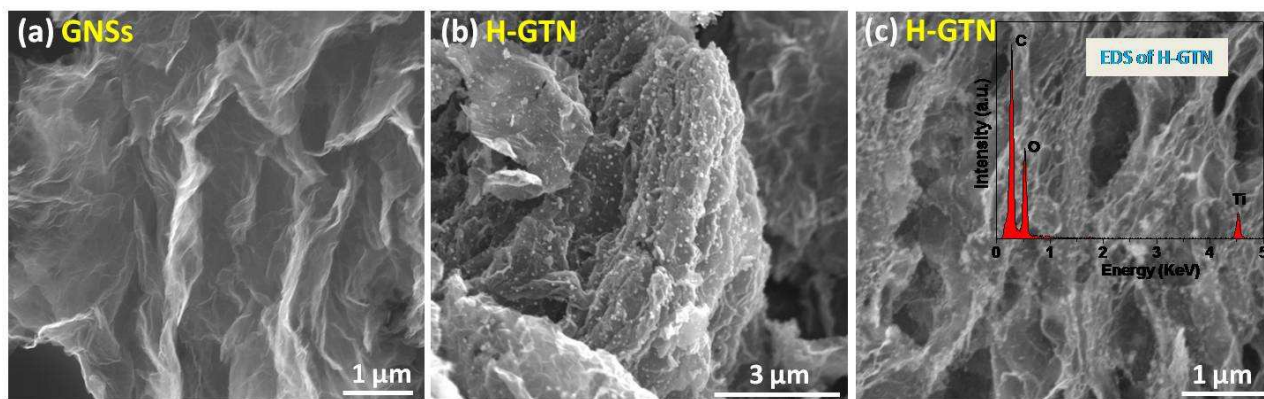


**Fig./Scheme XX Fig. 2** SEM image of (a) GNSs and (b, c) H-GTN.

The EDS analysis of the H-GTN hybrid shows the presence of C, O, and Ti elements. The existence of Ti and O with an approximate ratio of 1:2 implies its stoichiometry. The TEM and HRTEM images of as-synthesized GNSs and H-GTN are shown in Fig. 3. It is clearly seen from Fig. 3a that GNSs are transparent with wrinkles on the surface. The HRTEM images of GNSs (Fig.

3b) show the few layer graphene and the number of layers varies between 4-7 layers. Fig. 3c shows anchored and nicely distributed TiO$_2$ nanoparticles on the GNSs and anchored on the graphene sheets. Due to the homogeneous distribution, the aggregation of TiO$_2$ nanoparticles or the GNSs is prohibited and the specific surface area of TiO$_2$ is highly increased.

# Journal Name

# ARTICLE TYPE
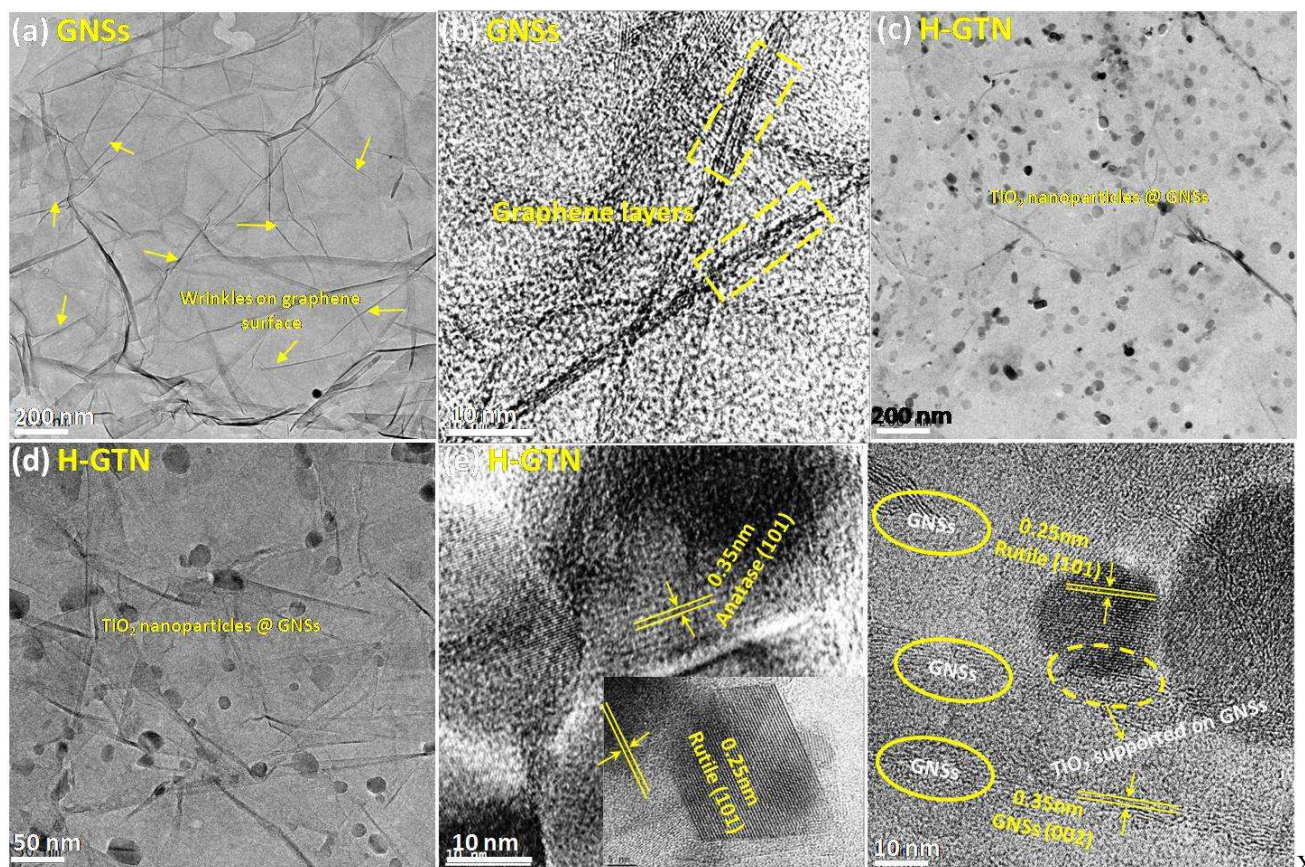


**Fig. 3** TEM micrographs of as synthesized (a) GNSs, (b) HRTEM of GNSs, (c, d) H-GTN and (e, f) HRTEM of H-GTN with different lattice plane orientations.

This is beneficial for fast diffusion of the redox phase, which
5 makes the hybrid to attain high electrochemical capacitance. The
adjacent lattice spacing as shown in Fig. 3d corresponds to the
distance between the two nearest crystal planes of GNSs and
$TiO_2$ as clearly observable in the higher magnification image. The
HRTEM images (Fig. 3e,f) of H-GTN show the lattice fringes of
10 spacing 0.37, 0.35 and 0.25 nm, that correspond to (002) crystal
plane of GNSs, (101) plane of anatase $TiO_2$ and (101) plane of
rutile $TiO_2$, respectively. The clear lattice plane of $TiO_2$ indicates
that the $TiO_2$ is of high crystallinity.

The XRD pattern of the as-synthesized GNSs and H-GTN
15 are shown in Fig. 4. The peaks at $2\theta$ values of 25.3, 37.8, 48.0,
53.9, 55.1, 62.7, 68.8, 70.3, and 75.0° can be indexed to (101),
(004), (200), (105), (211), (204), (116), (220), and (215) crystal
planes of anatase $TiO_2$, resp. In addition, characteristic diffraction
peaks of rutile phase of $TiO_2$ at 27.4, 36.1, and 41.2° are also
20 observed, that are attributed to the (110), (101), and (111) faces.
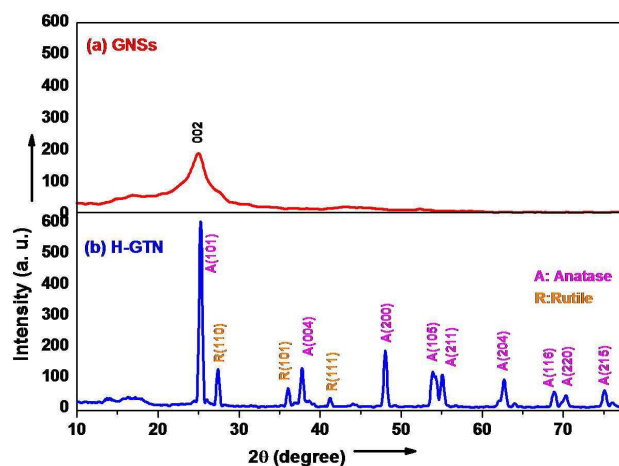


**Fig. 4** XRD pattern of (a) GNSs and (b) H-GTN.

Notably, no typical diffraction peaks of separate GNSs are observed in the H-GTN. There are some small intensity peaks present in the range of 13-20 deg, which are also noticeable in GNSs XRD pattern. These peaks show the presence of stacked GNSs in the sample. The most intense diffraction peak of GNSs may not be distinguishable as the same peak at ~25° (002) is overlapped or suppressed by the (101) diffraction peak of anatase $TiO_2$.[20, 21]

Bonding nature of GNSs and H-GTN was further investigated by Raman spectroscopy. Fig 5 shows the Raman spectra of GNSs and H-GTN. Both samples exhibit two peaks namely D-band and G-band. The D-band is associated with the presence of defects in the hexagonal graphitic layers and the G-bands is associated with Raman-active $E_{2g}$ mode which is usually assigned to the breathing mode of к point phonons of $A_{1g}$ symmetry and the $E_{2g}$ phonon of C $sp^2$ atoms, respectively.[22] It can be noted that the Raman D-band peak of GNSs at 1359 $cm^{-1}$ as been shifted to 1336 $cm^{-1}$ in H-GTN i.e. shifted towards lower wave number. Raman G-bands peak of GSs at 1583 $cm^{-1}$ has been shifted to 1587 $cm^{-1}$ in H-GTN i.e. shifted towards higher wave number. These observations show that the D-band is slightly red-shifted by 23 $cm^{-1}$ in the H-GTN, whereas the G band has shown a blue shift of 4 $cm^{-1}$. Similar shifts in the case of H-GTN have also been reported elsewhere.[23, 24] These shifts in the Raman peak have been attributed to the chemical interaction between GNSs and $TiO_2$ nanoparticles. The $I_D/I_G$ ratio has been found to increase from 0.48 to 0.92 for GNSs to H-GTN. This indicates the existence of reduction to graphene and interaction between graphene and $TiO_2$ nanoparticles.[25]
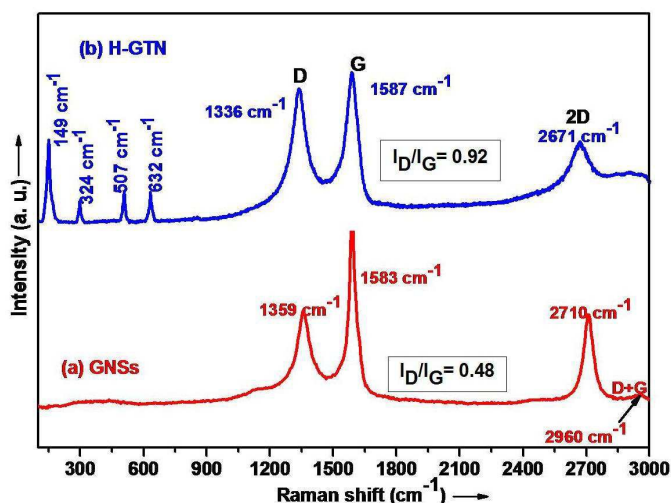
The second order Raman feature, the 2D-band at 2710 $cm^{-1}$ and D+G band at 2960 $cm^{-1}$ are very sensitive to the stacking order of the graphene sheets along the c-axis (the number of layers) and show more broadened shape (often a doublet) with an increasing number of graphene layers.[26, 27] The 2D peak position of the H-GTN (Fig. 5b) is shifted to 2671 $cm^{-1}$ from that of GNSs at 2710 $cm^{-1}$, which indicates formation of few layer graphene in $TiO_2$ in H-GTN.[28] The intensity ratio of D band to G band is usually used to represents the relative degree of disorder.[29] These disorderness are associated with vacancies, grain boundary and amorphous carbon presents in the as synthesized samples.[30] The intensity ratio of D band to G band, for H-GTN (0.92) shows an enhanced value compared to that for GNSs (0.48), suggesting the presence of more localized $sp^3$ defects within the $sp^2$ domains carbon network on H-GTN.[28] This is also an evidence of the reduction that take place during the formation of H-GTN. It suggests that the $TiO_2$ lattices are possibly entrapped inside the GNSs by concurring chemical reaction. In addition, peaks around 149 $cm^{-1}$ (the main $E_g$ anatase vibration mode), 324 $cm^{-1}$ ($B_{1g}$), 507 $cm^{-1}$ ($A_{1g}$), and 632 $cm^{-1}$ ($E_g$) $cm^{-1}$ suggest that the anatase crystallites are the major species in H-GTN. These signatures of anatase $TiO_2$ already has been reported in the Raman spectra of H-GTN.[31]

The Fourier transform infrared (FTIR) study of as-synthesized GNSs and H-GTN in the range of 4000-400 $cm^{-1}$ is shown in Fig. 6. The peaks at 3173 and 3389 $cm^{-1}$ are due to the presence of O-H stretching vibrations of the C-OH groups and water in GNSs and H-GTN. The other peaks in GNSs, correspond to carboxyl C=O (1728 $cm^{-1}$), aromatic stretching C=C (1627 $cm^{-1}$), tertiary C-OH group stretching (1376 $cm^{-1}$), and alkoxy C-OH group stretching vibrations (1070 $cm^{-1}$).[32]



**Fig. 5** Raman spectra of (a) GNSs and (b) H-GTN.
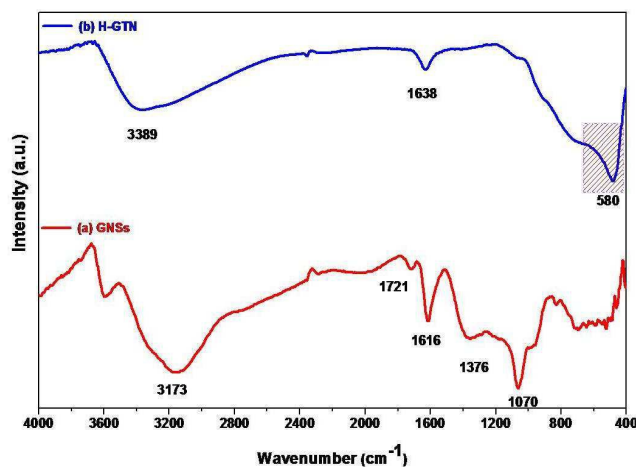


**Fig. 6** FTIR spectra of (a) GNSs and (b) H-GTN.

In H-GTN, the peak at 1638 cm$^{-1}$ correspond to C=C, which is shifted towards higher wave number side as comparison to GNSs. In Fig. 6b, compared with GNSs, the intensities of the peaks corresponding C=O and C-OH groups disappeared in the FTIR spectrum of H-GTN, indicating that the oxygen-containing functional groups in GNSs were removed from H-GTN. The broad band between 600 and 1000 cm$^{-1}$ is the characteristic of Ti–O–Ti stretching in H-GTN based materials.[33, 34] This peak could be ascribed to a combination of Ti-O-Ti and Ti-O-C vibration.[9, 35] The presence of Ti-O-C (580 cm$^{-1}$) bonds indicates the firmly bonding between the TiO$_2$ nanoparticles and GNSs during the hydrothermal process.

X-ray photoelectron spectroscopy (XPS) is carried out to evaluate the chemical composition of H-GTN sample. The typical XPS spectra of as prepared H-GTN sample are displayed in Fig. 7. As shown from Fig. 7a, the full scale XPS spectra show the C, O,and Ti photoelectron lines as detected in the XPS survey spectra of H-GTN.The Ti 2p spectrum (Fig.7b) showing the spin–orbit split lines of Ti 2p$_{3/2}$ and Ti 2p$_{1/2}$ located at 458.7 and 464.7 eV, respectively, that are characteristic of the Ti$^{4+}$ oxidation state.[36] The ratios (at%) of C, Ti, and O are 65.54 : 10.04 : 24.42, respectively**.** The O/Ti ratio is 2.43, (>2 of the stoichiometry of Titania) slightly higher than that of pristine TiO$_2$ nanoparticles, resulting from the additional oxygen containing functional group of the reduced graphene. In order to investigate the states of carbon in the sample, spectrum of the C 1s core levels were measured and shown in Fig.7d. Deconvolution of the C 1s peak in the XPS spectrum performed by four types of carbon bonds, namely, C-C (284.51 eV), C=C (284.84 eV), COOH (289.50) and C-O (285.95 eV).[37] The low intensity small peaks related to oxygenate C-O groups and very small amount of carboxyl group COOH indicate the presence of residual oxygenate groups on the H-GTN. The smaller peak corresponds to the oxygenate groups suggest a considerable de-oxygenation and the formation of H-GTN.[38]

A small amount of residual oxygenate groups on H-GTN are believed to be favorable for maintaining a good dispersion of the nanoparticles.
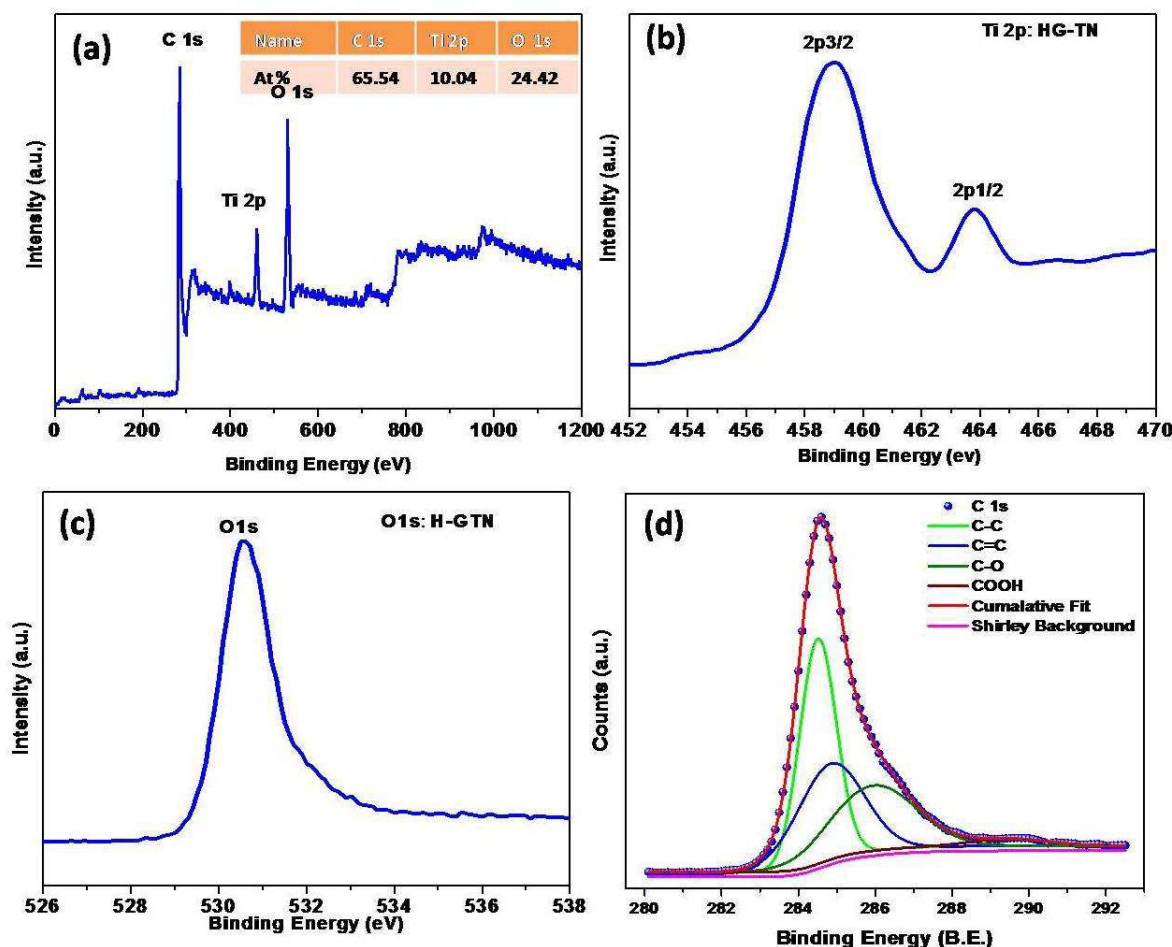


**Fig. 7** XPS survey spectra of (a) H-GTN. Core level XPS spectra of (b) Ti 2p, (c) O 1s and (d) C 1s of H-GTN.

# ARTICLE TYPE

In the process of simultaneous hydrothermal conversions of GO to graphene, the C-O functional groups on the surface of GO may react with [TiO] framework to form the Ti-O-C bonds, thus acting as the anchoring spots to initiate and support the growth of titania nanoparticles. In the O 1s spectrum (Fig.7c), the peak located at 531.1eV is attributed to O-H or the Ti-O-C groups.

Electron energy loss spectroscopy (EELS) was again carried out to confirm the presence of Ti-O-C group. The EEL spectra for GNSs and H-GTN are shown in Fig 8. This shows the presence of Ti and O together with C peaks. Each C- K edge EELS consists of a peak at around 295 eV due to excitations from the 1s level to empty $\pi^*$ states of the $sp^2$-bonded atoms. The H-GTN show that Ti and O elements result from anatase $TiO_2$ and C element results from the GNSs. O-K, Ti-$L_{2,3}$ and Ti-$L_1$ peaks occur at ~332, ~460 and ~560 eV, respectively.[39]
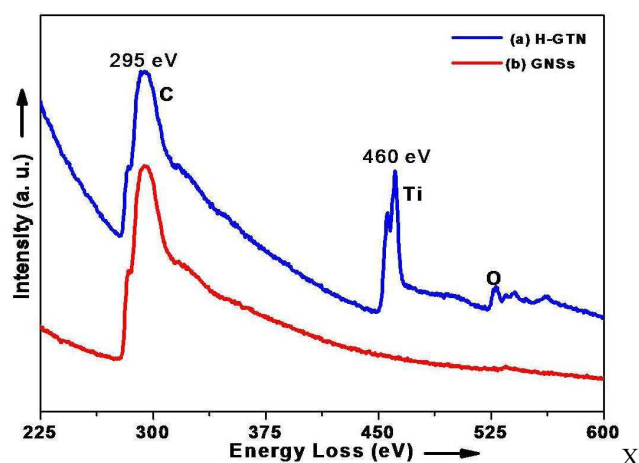


**Fig. 8** EEL spectra of (a) GNSs and (b) H-GTN.

Fig. 9a shows the photoluminescence (PL) of $TiO_2$ and H-GTN. PL spectra of H-GTN were measured by using an ultraviolet light with a 265 nm wavelength as the excitation source and the results are shown in Fig. 9a. A strong emission peak around 500 nm was observed, implying that most of charges quickly recombine in $TiO_2$ to produce PL emission. The H-GTN results show that nearly disappearance of PL intensities, which indicates that, the electron-hole recombination. When the pure $TiO_2$ nanoparticles were coupled with GNSs, electrons would flow from conduction band (CB) of $TiO_2$ into GNSs, leading to the formation of Schottky barrier at the H-GTN interface.[40]
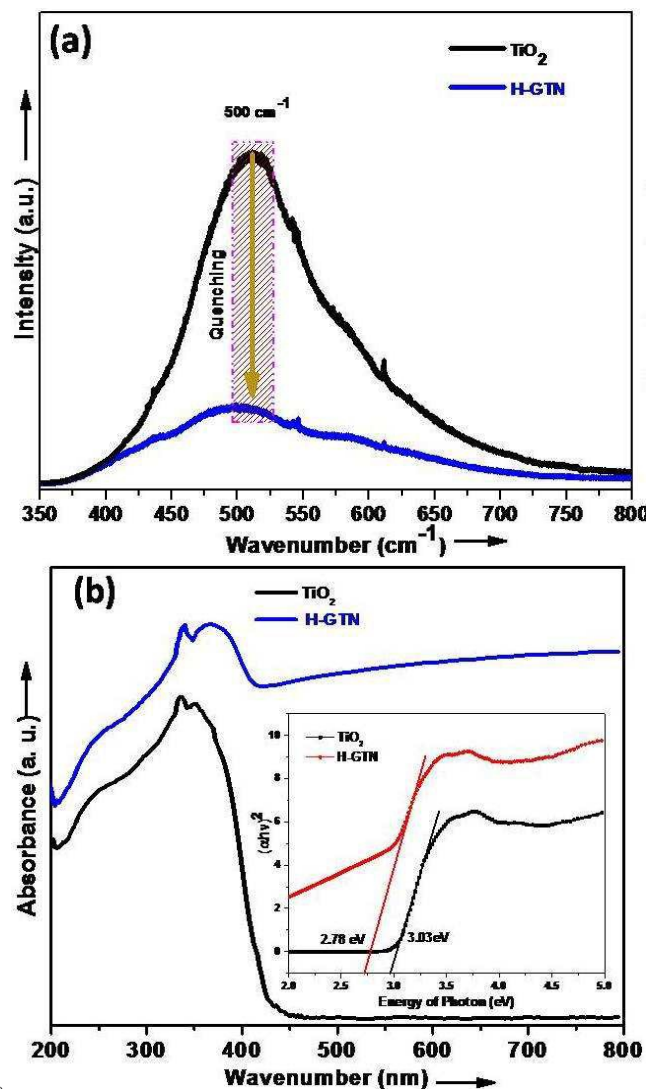


**Fig. 9** Optical properties of (a) PL spectra and (b) UV-visible of $TiO_2$ and H-GTN.

UV-visible spectrum for $TiO_2$ and H-GTN are shown in Fig. 9b. Fig. 9b shows that in the whole visible region of the spectrum, as observed for other carbonaceous materials, GNSs combined and attached with $TiO_2$ nanoparticles.[41-43] After the formation of H-GTN, a bit shift in the absorption edge into the visible light region was observed. An induced dramatically improved light absorption in the visible light region was also observed, along with noticeable red shift of *ca.* 171 nm in the absorption edge of H-GTN, compared to bare $TiO_2$. The red shift in the absorption band of HGTN may be attributed to the Ti-O-C bond. Ti-O-C bonds have the similar effect on $TiO_2$ as impurities or carbon

doping. The carbon doping or impurities in $TiO_2$ composite introduce defect states into the $TiO_2$ band gap, allowing photogeneration from lower-energy photons. The Ti–O–C bond in the HGTN is formed due to interaction of π electrons of the graphene nanosheets and free electrons in $TiO_2$ which results into the replacement of some Ti-O-Ti bond to Ti-O-C covalent bonds due to higher electronegativity of the C than Ti.[21,45] In fact, the graphene nanosheets might act as photosensitizer chemically bonded with $TiO_2$ through the interactions between Ti ions and oxygen groups and thus contributes to the visible light absorption. Compared to pure $TiO_2$ and H-GTN, the H-GTN exhibits increased spectra in UV region, suggesting that the electronic conjugation within the GNSs was restored upon chemical reduction.[44] The narrowing of the band gap of $TiO_2$ occurred with the introducing of GNSs. This narrowing should be attributed to the chemical bonding between $TiO_2$ and GNSs, that is the formation of Ti-O-C bond, similar to the case of others reports for graphene- $TiO_2$ composites.[9, 46] As shown in the inset of Fig. 9b, The optical band gap is for a semi-conductor near the absorption band edge can be estimated from the following equation known as the Tauc plot:[47]

$$(\alpha h v) \propto (h v - E_g)^n$$

Where α is the optical absorption coefficient, hv is the energy of the incident photon, $E_g$ the optical band and n = 0.5 and 2 correspond to direct allowed transition semiconductor and indirect allowed transition semiconductor respectively. Tauc plot has been drawn between $(\alpha h v)^2$ and energy of the photon for the calculation of the optical bandgap of $TiO_2$ and H-GTN.[48] Due to mixed phase Anatase (3.2 eV) and Rutile (3.0 eV) and some impurities phases present in TiO2 causes the measured optical bandgap lower than the standard value of the Anatase Phase 3.2 eV. The band gap of $TiO_2$ was decreased from 3.03 eV to 2.78 eV by uniformly decoration of $TiO_2$ nanoparticles. Fig. 9b shows that after hybridization with GNSs, the adsorption edges of $TiO_2$ was shifted to visible light region.

To further evaluate the potential application of the H-GTN hybrids as electrode materials for electrochemical supercapacitors, cyclic voltammetry (CV) measurements were carried out between 0 and 0.6 V (vs. Ag/AgCl) at various scan rates ranging from 3 to 70 mV/s, and corresponding specific capacitance has been shown in Fig. 10a. The specific capacitances of electrodes were calculated using CV curve using following equations as given below

$$c = \frac{\int I dv}{v \times m \times \Delta V}$$

where C is the specific capacitance based on the mass of electroactive materials (F/g), $\int I dv$ is the integrated area of CV curve, I is the response current density (A/g), $v$ is the scan rate (mV/s), $m$ is the mass of the electroactive materials in the electrode (g), $\Delta V$ is the sweep potential window (V). The measurements were carried out in a 0.5 M BMIM-BF$_4$ /CH$_3$CN solution as electrolyte at room temperature. The specific capacitances evaluated from the CV curves were 531, 470, 431, 404, 403, 404, 402, 401, and 401 F/g at scan rates of 3, 5, 10, 20, 30, 40, 50, 70 and 100 mV/s respectively as shown in Fig. 10 b. The specific capacitance shows nearly stable capacitance of 400 F/g above 20 mV/s which is more stable and constant as reported by other groups.[49]

We observed that the specific capacitance for both electrodes decreased with an increase in the scan rate from 3 to 100mV/s. This is a common phenomenon and is caused by the insufficient time available for ion diffusion and adsorption inside the smallest pores within a particle at high scan rates.[50] For high scan rates, the diffusion rates of electrolyte ions are limited by electrode structural properties, and only the external sites can take part in ion transfer reaction. But for low scan rates, all the active areas, including external and internal surfaces, can be utilized for charge/discharge and electrochemical utilization of $TiO_2$ nanoparticles. The improvement can probably be attributed to the unique structure of H-GTN. The $TiO_2$ nanoparticles, are well dispersed on the surface of GNSs not only effectively inhibit the stacking/agglomerating of GNSs, but also improve the electrochemical utilization of H-GTN. GNSs also provide a highly conductive network for electron transport during the charge/discharge processes. The excellent interfacial contact and increased contact area between $TiO_2$ and GNSs can significantly improve the accessibility of H-GTN to the electrolyte ions and shorten the ion diffusion and migration pathways. Furthermore, GNSs can also serve as reliable conductive channels between individual active $TiO_2$ nanoparticles. The cycle life time of H-TGN electrode was examined. As shown Fig. 10 c, the cyclic stability test displays insignificant decrease in the specific capacitance over 100 cycles, approximately 9.1% from of the initial value and after 100 cycle its shows the nearly stable behavior.

# ARTICLE TYPE
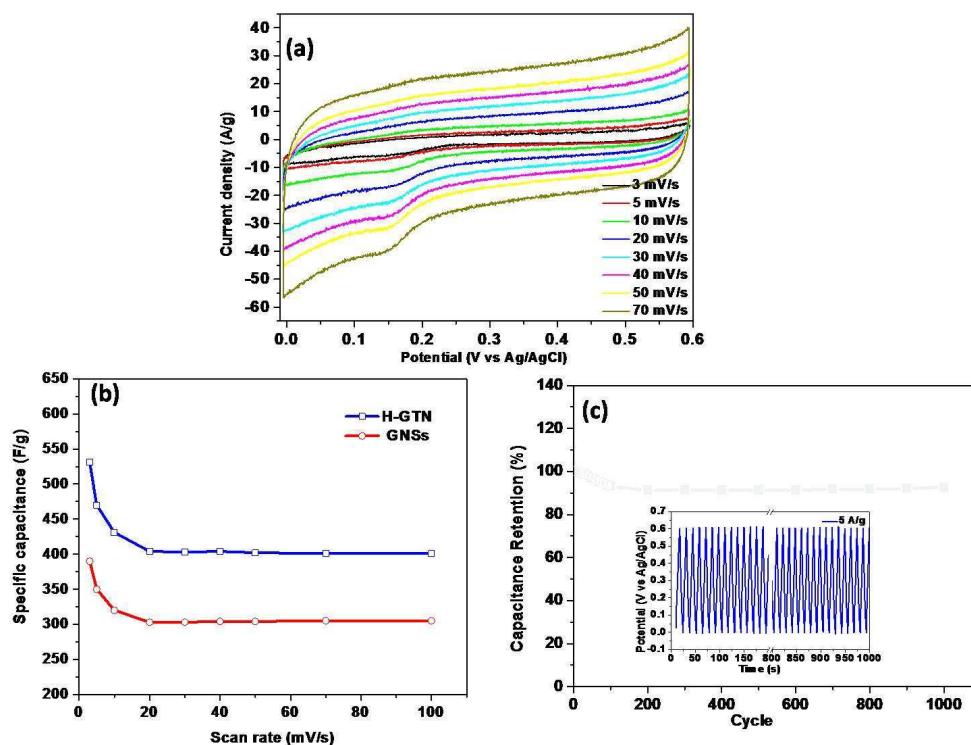


**Fig. 10** Electrochemical measurements of H-GTN. (a) CV curve of H-GTN (b) specific capacitance values of H-GTN with scan rates and (c) Long-term cycling stability of the supercapacitor at a constant current density of 5 A/g over 1000 cycles; the inset shows charge/discharge curve of the H-GTN in the potential range from 0 to 0.6 V at 5A/g.

5 This demonstrates the excellent electrochemical performance of the H-GTN electrode material for application in practical energy storage devices. It is concluded that the synergistic effect between conducting GNSs and $TiO_2$ nanoparticles is responsible for the excellent electrochemical 10 performance of the process.

## Experimental Methods

### Synthesis of Graphene oxide

Graphene oxide was prepared from graphite by modified Hummer's method.[51] The graphite powder (1 g) was dispersed in 15 concentrated sulphuric acid ($H_2SO_4$) (25 mL, 98 wt. %) containing sodium nitrate (1 g, $NaNO_3$), and then, potassium permanganate ($KMnO_4$, 5 g) were slowly added with continuous vigorous stirring and cooling in ice bath to prevent the exceeding temperature. The ice bath was removed and replaced by a water 20 bath, and the mixture was heated to 40 $^o$C for 1 h for releasing gas under continuous stirring, followed by slow addition of deionized (DI) water (50 mL), which produced a rapid temperature increase in solution. The reaction was maintained for 24h in order to increase the oxidation degree of the graphene 25 oxide. The resultant brown-yellow suspension was terminated by addition of more DI water (300 mL), followed by a hydrogen peroxide solution ($H_2O_2$, 30%, 10 mL). The solid product was separated by centrifugation and washed with 500 mL of 1:5 HCl solution, and water until pH = 7 was achieved. Finally, the 30 powder was dried at room temperature. This dried powder was thermally exfoliated in argon (Ar) atmosphere at 1000 $^0$C for the conversion into graphene nanosheets (GNSs).

### Synthesis of hybrid graphene-TiO$_2$ Nanostructure (H-GTN)

In a typical synthesis route for H-GTN, GNSs (50 mg) and 35 titanium tetraisopropoxide ($TiC_{12}H_{28}O_4$) (7 mg which was optimised after several experiments) were added to 50 mL of DI water and then the solution was sonicated for 45 min and stirred for 1 h using magnetic stirrer, respectively. The electrostatic and molecular grafting between GNSs and $TiC_{12}H_{28}O_4$ was 40 accomplished by stirring the mixture for 1 h at room

temperature.[52] After complete stirring, the solution was transferred into a 100 mL Teflon-lined tightly sealed stainless steel autoclave. The autoclave was then heated to 240 °C and kept there for 36 h. After the complete hydrothermal treatment, the hybrid nanostructure, denoted as H-GTN, was centrifuged, washed, and finally dried in air at 55 °C overnight.

### Materials characterization

The as grown materials were characterized by X-ray diffractmeter (XRD, Philips 1710). The sample was scanned for $2\theta$ from $10^o$ to $80^o$. Scanning electron microscope (SEM) observations were performed using a Philiphs XL 20 at 2kV in gentle-beam mode without any metal coating with the fully dried sample loaded on a carbon tape. The X-ray photoelectron spectroscopy (XPS) spectrum was recorded on a MultiLab2000 photoelectron spectrometer (Thermo- VG Scientific, USA) with Al K$\alpha$ (1486.6 eV) as the X-ray source. All XPS spectra were corrected using the C 1s line at 284.6 eV. The EDS analysis was performed at several points in the region and averaged to obtain the representative results. The transmission electron microscopy (TEM) analysis was carried out using a Tecnai G$^2$ 20 microscope operated at 200 kV using a holey carbon-coated copper grid. The sample was prepared by dispersing a small amount of dry powder in ethanol or water. Then, one droplet of the suspension was dropped on a holey-carbon coated, 300 mesh copper TEM grids and allowed to dry in air at room temperature. The Raman spectrum was acquired on a LabRAM HR UV/vis/NIR (Horiba JobinYvon, France) using a CW Ar-ion laser (514.5 nm) as an excitation source focused through a confocal microscope (BXFM, Olympus, Japan) equipped with an objective lens (50×, numerical aperture = 0.50) at room temperature. The changes in the surface chemical bonding and surface composition were characterized by Fourier transform infrared spectroscopy (FT-IR, Jasco FT-IR 4100). The test samples were pressed into tablets with KBr. The UV-visible absorption spectra were recorded using a (Jasco,V-570) spectrometer. The photoluminescence (PL) emission spectra of the samples were recorded on a fluorescence spectrophotometer (LabRAM HR UV/Vis/NIR PL) using a 325 nm He-Cd laser as an excitation light source. Electron energy loss spectroscopy (EELS) spectra were recorded on a JEOL (TEM: ARM 200F) microscope operated at 300 using holey carbon-coated copper grid.

### Electrochemical Measurements

All electrochemical measurements were done in a three-electrode system. The H-GTN electrode behave as working electrode, Pt (platinum) wire as a counter electrode, and Ag/AgCl electrode as a reference electrode. Electrochemical measurements, such as cyclic voltammetry (CV) were carried out by a VersaSTAT 3 (Princeton Applied research). The glassy carbon electrodes (GCEs) (5 mm diameter) were polished first with 1.0 and 0.05 μm alumina slurry. Then, 1.0 mg of the H-GTN hybrid material was dispersed in 1.0 ml of dimethylformamide (DMF) with the aid of ultrasonicator to give a 1.0 mg/mL black suspension. Then, 10 μL of the black suspension was dropped on a cleaned GCE electrode with the help of a micro-syringe and the solvent was evaporated in air. Thus, a uniform film of H-GTN hybrids coating was formed on the surface of GCE. Finally, 5 μL of Nafion (5 wt.%) was cast and used as a net to stably hold the H-GTN hybrids on the electrode surface. The solvent was allowed to evaporate before use. The final electrode was taken as the H-GTN hybrid electrode. All electrochemical measurements were done with a three-electrode system, which set the above working electrode, Pt (platinum) wire as a counter electrode, and Ag/AgCl electrode as a reference electrode.

## Conclusions

Uniformly dispersed $TiO_2$ nanoparticles on the graphene surfaces were achieved by a new, straightforward and facile one pot route by in situ hydrothermal method. Mixed rutile and anatase phases $TiO_2$ sphere like nanoaprtciles were homogeneously dispersed on the few layers GNSs. Nanoparticles had a narrow size particle distribution of ~10-20 nm. The graphene evidently influenced the formation of $TiO_2$ and made the nanoparticles more uniform in morphology and size due to the selective nucleation and growth of $TiO_2$ on GNSs. We observed the optical properties of $TiO_2$ nanoparticles to be directly affected by GNSs and the photoluminescence spectra of H-GTN attributed the significant improvement in quenching with respect to $TiO_2$ nanoparticles in the wavelength of 400-700 nm. UV-visible spectra showed the slight decrease in band gap after the formation of H-GTN. The electrochemical measurements results showed that GNSs and $TiO_2$ nanoparticles enhanced the electrode conductivity, stability and improved the supercapacitive behavior of H-GTN. Significantly, this result also showed that the H-GTN had a high specific capacitance with constant stability at high scan rate and long cycling stability. The present as synthesized materials suggested that the H-GTN can be used as a promising material for supercapacitor for high performance.

## Notes and references

*aDepartment of Materials Science and Engineering, Yonsei University, Seoul-120749, South Korea; E-mail:rajeshbhu1@gmail.com*
*bDepartment of Physics, Banaras Hindu University, Varanasi-221005, India*
*cDepartment of Physics, Indian Institute of Technology (Banaras Hindu University), Varanasi-221005, India; E-mail: rksbhu@gmail.com*
*dNanotechnology Application Centre, Faculty of Science, University of Allahabad, Allahabad-211002, India; E-mail: dubey.pawan@gmail.com*
*eAvenida Ecuador 3493, Estación Central, Departamento de Física, Universidad de Santiago de Chile, Santiago-9170124, ChileE-mail:* dineshpsingh@gmail.com
*Dept Of Physics, VSSD (PG) College, Kanpur, India-208002, **Email:** rmanohar28@gmail.com*

## References

1. A. A. Balandin, S. Ghosh, W. Bao, I. Calizo, D. Teweldebrhan, F. Miao and C. N. Lau, *Nano Letters*, 2008, **8**, 902.
2. K. I. Bolotin, K. J. Sikes, Z. Jiang, M. Klima, G. Fudenberg, J. Hone, P. Kim and H. L. Stormer, *Solid State Communications*, 2008, **146**, 351.
3. M. D. Stoller, S. Park, Y. Zhu, J. An and R. S. Ruoff, *Nano Letters*, 2008, **8**, 3498.
4. C. Lee, X. Wei, J. W. Kysar and J. Hone, *Science*, 2008, **321**, 385.
5. Y. Xuan, Y. Q. Wu, T. Shen, M. Qi, M. A. Capano, J. A. Cooper and P. D. Ye, *Applied Physics Letters*, 2008, **92**, 013101.
6. T. Kuila, A. K. Mishra, P. Khanra, N. H. Kim and J. H. Lee, *Nanoscale*, 2013, **5**, 52.
7. B. F. Machado and P. Serp, *Catalysis Science & Technology*, 2012, **2**, 54.
8. H. Kim, A. A. Abdala and C. W. Macosko, *Macromolecules*, 2010, **43**, 6515.
9. H. Zhang, X. Lv, Y. Li, Y. Wang and J. Li, *ACS Nano*, 2009, **4**, 380.
10. A. K. Mishra and S. Ramaprabhu, *The Journal of Physical Chemistry C*, 2011, **115**, 14006.
11. M. Toupin, T. Brousse and D. Bélanger, *Chemistry of Materials*, 2004, **16**, 3184.
12. H. Kim and B. N. Popov, *Journal of Power Sources*, 2002, **104**, 52.
13. C.-C. Hu, K.-H. Chang, M.-C. Lin and Y.-T. Wu, *Nano Letters*, 2006, **6**, 2690.
14. Y.-T. Wang, A.-H. Lu, H.-L. Zhang and W.-C. Li, *The Journal of Physical Chemistry C*, 2011, **115**, 5413.
15. C. Xu, X. Wang and J. Zhu, *The Journal of Physical Chemistry C*, 2008, **112**, 19841.
16. G. Williams, B. Seger and P. V. Kamat, *ACS Nano*, 2008, **2**, 1487.
17. P.-C. Chen, G. Shen, Y. Shi, H. Chen and C. Zhou, *ACS Nano*, 2010, **4**, 4403.
18. D. Wang, D. Choi, J. Li, Z. Yang, Z. Nie, R. Kou, D. Hu, C. Wang, L. V. Saraf, J. Zhang, I. A. Aksay and J. Liu, *ACS Nano*, 2009, **3**, 907.
19. C. Zhu, S. Guo, P. Wang, L. Xing, Y. Fang, Y. Zhai and S. Dong, *Chemical Communications*, 2010, **46**, 7148.
20. J. S. Chen, Z. Wang, X. C. Dong, P. Chen and X. W. Lou, *Nanoscale*, 2011, **3**, 2158.
21. Y.-J. Xu, Y. Zhuang and X. Fu, *The Journal of Physical Chemistry C*, 2010, **114**, 2669.
22. W. Zhang, J. Cui, C.-a. Tao, Y. Wu, Z. Li, L. Ma, Y. Wen and G. Li, *Angewandte Chemie International Edition*, 2009, **48**, 5864.
23. Y. Min, K. Zhang, W. Zhao, F. Zheng, Y. Chen and Y. Zhang, *Chemical Engineering Journal*, 2012, **193–194**, 203.
24. O. Akhavan, M. Abdolahad, A. Esfandiar and M. Mohatashamifar, *The Journal of Physical Chemistry C*, 2010, **114**, 12955.
25. H. Gao, W. Chen, J. Yuan, Z. Jiang, G. Hu, W. Shangguan, Y. Sun and J. Su, *International Journal of Hydrogen Energy*, DOI: http://dx.doi.org/10.1016/j.ijhydene.2013.01.155.
26. M. A. Pimenta, G. Dresselhaus, M. S. Dresselhaus, L. G. Cancado, A. Jorio and R. Saito, *Physical Chemistry Chemical Physics*, 2007, **9**, 1276.
27. A. C. Ferrari, J. C. Meyer, V. Scardaci, C. Casiraghi, M. Lazzeri, F. Mauri, S. Piscanec, D. Jiang, K. S. Novoselov, S. Roth and A. K. Geim, *Physical Review Letters*, 2006, **97**, 187401.
28. D. Graf, F. Molitor, K. Ensslin, C. Stampfer, A. Jungen, C. Hierold and L. Wirtz, *Nano Letters*, 2007, **7**, 238.
29. A. C. Ferrari and J. Robertson, *Physical Review B*, 2000, **61**, 14095.
30. T. A. Pham, B. C. Choi, K. T. Lim and Y. T. Jeong, *Applied Surface Science*, 2011, **257**, 3350.
31. Y. Lei, L. D. Zhang and J. C. Fan, *Chemical Physics Letters*, 2001, **338**, 231.
32. S. Stankovich, D. A. Dikin, R. D. Piner, K. A. Kohlhaas, A. Kleinhammes, Y. Jia, Y. Wu, S. T. Nguyen and R. S. Ruoff, *Carbon*, 2007, **45**, 1558.
33. K. Zhou, Y. Zhu, X. Yang, X. Jiang and C. Li, *New Journal of Chemistry*, 2011, **35**, 353.
34. J. Shen, B. Yan, M. Shi, H. Ma, N. Li and M. Ye, *Journal of Materials Chemistry*, 2011, **21**, 3415.
35. S. Sakthivel and H. Kisch, *Angewandte Chemie International Edition*, 2003, **42**, 4908.
36. S.-K. Joung, T. Amemiya, M. Murabayashi and K. Itoh, *Chemistry – A European Journal*, 2006, **12**, 5526.
37. N. Yang, J. Zhai, D. Wang, Y. Chen and L. Jiang, *ACS Nano*, 2010, **4**, 887.
38. S. Stankovich, R. D. Piner, X. Chen, N. Wu, S. T. Nguyen and R. S. Ruoff, *Journal of Materials Chemistry*, 2006, **16**, 155.
39. F. Zou, Y. Yu, N. Cao, L. Wu and J. Zhi, *Scripta Materialia*, 2011, **64**, 621.
40. T. Kamegawa, D. Yamahana and H. Yamashita, *The Journal of Physical Chemistry C*, 2010, **114**, 15049.
41. C. G. Silva and J. L. Faria, *Applied Catalysis B: Environmental*, 2010, **101**, 81.
42. S. Shanmugam, A. Gabashvili, D. S. Jacob, J. C. Yu and A. Gedanken, *Chemistry of Materials*, 2006, **18**, 2275.
43. L. Zhang, P. Liu and Z. Su, *Journal of Molecular Catalysis A: Chemical*, 2006, **248**, 189.
44. P. Cheng, Z. Yang, H. Wang, W. Cheng, M. Chen, W. Shangguan and G. Ding, *International Journal of Hydrogen Energy*, 2012, **37**, 2224.
45. M Xing, F Shen, B Qiu and J. Zhang , *Scientific Reports* 4 : 6341, (2014)
46. Y. Zhang, Z.-R. Tang, X. Fu and Y.-J. Xu, *ACS Nano*, 2010, **4**, 7303.
47. H. Jia, H. Xu, Y. Hu, Y. Tang, and L. Zhang, Electrochem. Commun. 9, 354 (2007).
48. J. Tauc, J. Mater. Res. Bull. 5, 721 (1970).
49. H. Su, T. Wang, S. Zhang, J. Song, C. Mao, H. Niu, B. Jin, J. Wu and Y. Tian, *Solid State Sciences*, 2012, **14**, 677.
50. J. Yan, T. Wei, W. Qiao, B. Shao, Q. Zhao, L. Zhang and Z. Fan, *Electrochimica Acta*, 2010, **55**, 6973.
51. W. S. Hummers and R. E. Offeman, *Journal of the American Chemical Society*, 1958, **80**, 1339.
52. Y.-B. Tang, C.-S. Lee, J. Xu, Z.-T. Liu, Z.-H. Chen, Z. He, Y.-L. Cao, G. Yuan, H. Song, L. Chen, L. Luo, H.-M. Cheng, W.-J. Zhang, I. Bello and S.-T. Lee, *ACS Nano*, 2010, **4**, 3482.